Cobalt Hexammine Inhibition of the Hammerhead Ribozyme†

Thomas E. Horton and Victoria J. DeRose*

Department of Chemistry, Texas A&M University, College Station, Texas 77842-3012

Received May 19, 2000; Revised Manuscript Received July 6, 2000

ABSTRACT: The effects of $Co(NH_3)_6^{3+}$ on the hammerhead ribozyme are analyzed using several techniques, including activity measurements, electron paramagnetic resonance (EPR), and circular dichroism (CD) spectroscopies and thermal denaturation studies. $Co(NH_3)_6^{3+}$ efficiently displaces Mn^{2+} bound to the ribozyme with an apparent dissociation constant of $K_{d\ app} = 22 \pm 4.2\ \mu M$ in 500 μM Mn^{2+} (0.1 M NaCl). Displacement of Mn^{2+} coincides with $Co(NH_3)_6^{3+}$ inhibition of hammerhead activity in 500 μM Mn^{2+}, reducing the activity of the WT hammerhead by ~15-fold with an inhibition constant of $K_i = 30.9 \pm 2.3\ \mu M$. A residual 'slow' activity is observed in the presence of $Co(NH_3)_6^{3+}$ and low concentrations of Mn^{2+}. Under these conditions, a single Mn^{2+} ion remains bound and has a low-temperature EPR spectrum identical to that observed previously for the highest affinity Mn^{2+} site in the hammerhead ribozyme in 1 M NaCl, tentatively attributed to the A9/G10.1 site [Morrissey, S. R., Horton, T. E., and DeRose, V. J. (2000) *J. Am. Chem. Soc. 122,* 3473−3481]. Circular dichroism and thermal denaturation experiments also reveal structural effects that accompany the observed inhibition of cleavage and Mn^{2+} displacement induced by addition of $Co(NH_3)_6^{3+}$. Taken together, the data indicate that a high-affinity $Co(NH_3)_6^{3+}$ site is responsible for significant inhibition accompanied by structural changes in the hammerhead ribozyme. In addition, the results support a model in which at least two types of metal sites, one of which requires inner-sphere coordination, support hammerhead activity.

The hammerhead ribozyme represents one of the best-characterized metalloribozymes to date. The importance of divalent cations in the site-specific phosphodiester bond cleavage is well documented (*1, 2*), but the exact nature of the metal−RNA interactions that promote this activity is still unclear. Hammerhead activity is believed to be facilitated by interactions of one or more divalent cation(s) whose roles include folding and chemistry (*1*−*6*).

$Co(NH_3)_6^{3+}$ is roughly the same ionic radius as magnesium(II) hexahydrate (*7*), but in $Co(NH_3)_6^{3+}$ the ammine ligands do not exchange with solvent, thereby preventing inner-sphere interactions with functional groups on the RNA. These properties make $Co(NH_3)_6^{3+}$ a useful probe in identifying the types of metal−RNA interactions required for ribozyme activity (*8*−*10*). $Co(NH_3)_6^{3+}$ has been used in RNA studies as a crystallographic heavy-atom replacement and as an exchange-inert NMR probe for the spectroscopically silent Mg^{2+} ion (*11*−*18*). In general, these studies show $Co(NH_3)_6^{3+}$ binding to regions that are also associated with Mg^{2+} sites, although the coordination details may not be the same for the two ions. $Co(NH_3)_6^{3+}$ was found to bind to an RNA pseudoknot (*18*) with an approximately 10−15-fold increase in affinity in comparison to Mg^{2+}, causing a significant stabilization as measured by thermal denaturation experiments. While $Co(NH_3)_6^{3+}$ has been reported to have significant structural effects on double-stranded DNA (*19*), similar observations for RNA have not been thoroughly characterized.

The effects of $Co(NH_3)_6^{3+}$ on hammerhead activity have not been thoroughly characterized (*20*). Lilley and co-workers have reported that low concentrations of $Co(NH_3)_6^{3+}$ block a folding event (*20*) predicted to include formation of the CUGA turn in the hammerhead core (*5*). Inhibition of hammerhead activity has been reported upon addition of other trivalent cations (*21*−*23*). Tb^{3+} and Eu^{3+} are thought to associate via inner-sphere contacts to the binding face of G5, possibly inhibiting hammerhead activity by blocking a conformational change associated with the transition state (*21, 22*).

Previously, we described the use of EPR[1] to measure the numbers and affinities of Mn^{2+} bound to a RNA/DNA hybrid hammerhead ribozyme (*24*). In a similar study, Hunsicker and DeRose (*25*) measured the relative affinities of several divalent cations to the hammerhead ribozyme by competition with Mn^{2+}. These studies show that the hammerhead has a population of 3−4 high-affinity Mn^{2+} sites ($K_d \sim 4\ \mu M$). RNA ligands associated with the highest affinity Mn^{2+} site were explored using electron spin−echo envelope modulation (ESEEM) and electron nuclear double resonance (ENDOR) spectroscopy (*26, 27*). The ligands identified by these techniques correlate well with those proposed for the A9/G10.1 site identified crystallographically in the junction of the conserved core and stem II of the hammerhead (*28, 29*).

† This work was supported by the NSF (CAREER to V.J.D., CHE-8912763 for Texas A&M University EPR facilities), the NIH (GM58096), and the Texas Higher Education Advanced Research Program. V.J.D. is a Cottrell Scholar of the Research Corporation.

* Corresponding author. Phone: 979-862-1401. Fax: 979-845-4719. Email: derose@mail.chem.tamu.edu.

[1] Abbreviations: EPR, electron paramagnetic resonance; ESEEM, electron spin−echo envelope modulation; ENDOR, electron nuclear double resonance; TEA, triethanolamine; t_m, melting temperature.

10.1021/bi001141g CCC: $19.00
Published on Web 08/18/2000

The A9/G10.1 metal binding site is required for hammerhead activity (*4, 31, 32*). The reason for the importance of this site is not clear due to its distance from the cleavage site observed crystallographically (>15 Å). The metal ion bound at the A9/G10.1 site has recently been predicted to be directly involved in the catalytic mechanism of the hammerhead ribozyme (*4, 31, 32*) by gaining additional ligands from the cleavage site in the transition state of the reaction (*4, 31*). This conclusion would require a significant rearrangement of the RNA tertiary structure, as predicted by X-ray crystallography (*33*), to facilitate the close approach of this site to the cleavage site. Since the metal binding site at A9/G10.1 includes inner-sphere contacts, it is expected that using the exchange-inert $Co(NH_3)_6^{3+}$ in competition and activity studies may provide further insight into the potential interactions at this site.

This paper attempts to further clarify the metal ion interactions that are required by the hammerhead ribozyme using the ligand-exchange-inert trivalent cation $Co(NH_3)_6^{3+}$. Activity measurements and Mn^{2+} competition studies are used to evaluate the effects of $Co(NH_3)_6^{3+}$ on hammerhead activation and metal binding. Additionally, circular dichroism and thermal denaturation studies were carried out in an attempt to elucidate potential structural effects caused by $Co(NH_3)_6^{3+}$, and their relationship to hammerhead activity.

MATERIALS AND METHODS

RNA Synthesis and Purification. The 34 nucleotide enzyme strands were synthesized by in vitro transcription using T7 RNA polymerase as previously described (*34*). RNA transcription reactions were purified and dialyzed according to the procedures described in Horton et al. (*24*). The 2′-O-Me and the unmodified 13 nucleotide substrate strands were purchased from Dharmacon Research (Boulder, CO) and purified as above. $Co(NH_3)_6^{3+}$ was purchased from Aldrich Chemical (99.999% pure) and used without further purification.

Metal-Binding Titrations Based on Mn^{2+} EPR Signal Amplitudes. Mn^{2+} binding to the RNA/RNA O-Me hybrid was measured as previously described (*24*).

Room-temperature EPR measurements were performed on an X-Band Bruker ESP-300 spectrometer with the following acquisition parameters: 0.2 mW microwave power, 26 G modulation amplitude, 6.1 G/s scan rate, average of 1−5 scans. Data were fit to a simple model of two sets of noninteracting sites (*24*).

EPR Measurements of Mn^{2+} Displacement. Intensities of Mn^{2+} EPR signals in the presence of 500 μM Mn^{2+} and 10 μM hybrid were measured as a function of added $Co(NH_3)_6^{3+}$ (10 μM−10 mM) and quantified as previously described (*24*). The data were then fit using a simple model that makes no assumptions about the numbers of ions involved in the displacement of a given number of Mn^{2+} ions (eq 1).

$$Mn^{2+}_{\text{released}} = \frac{a \times [Co(NH_3)_6^{3+}]}{(K_{\text{d app}} + [Co(NH_3)_6^{3+}] + b)} \qquad (1)$$

In eq 1, a is equal to the total change in Mn^{2+} bound and b is equal to the number of Mn^{2+} ions bound at the beginning of the titration. $K_{\text{d app}}$ equals the apparent dissociation constant for $Co(NH_3)_6^{3+}$ in 500 μM Mn^{2+} (0.1 M NaCl).

Measurements of Hammerhead Ribozyme Activity. Activities and rate constants were determined as previously described (*24*). Competition rates were carried out with 500 μM $MnCl_2$ and varying amounts of $Co(NH_3)_6^{3+}$, which were added together to the RNA/RNA hybrid to initiate the reaction. For these studies, a final hybrid concentration of 3 μM (spiked with ~200 nM ^{32}P substrate) was used in order to allow direct comparison with the results obtained by EPR. The reaction time courses were terminated by addition of 50 mM EDTA/8 M urea. The reaction mixture was then loaded on a 20% denaturing polyacrylamide gel and separated. Labeled substrate was visualized and quantitated by phosphorimaging analysis (Fuji).

Low-Temperature EPR Experiments. EPR data were obtained on a Bruker X-band ESP-300 spectrometer at 10 K. Samples were prepared in standard buffer with 20% ethylene glycol as a cryoprotectant (*27*) and a concentration of 500 μM RNA/RNA (O-Me) hybrid.

Thermal Denaturation Experiments. RNA denaturation experiments were carried out on a Cary 1 double-beam UV−Vis spectrometer equipped with a variable temperature controller. The sample concentration was 3 μM RNA. After annealing by heating to 90 °C for 90 s and cooling on ice, the appropriate amount of divalent cation was added from stock solutions in water. Samples were then loaded at room temperature into sealed cuvettes and placed in the spectrometer, which equilibrates to 4 °C for 30 min before starting the experiment. Data were collected at 0.3 and 0.7 °C intervals from 4 to 100 °C as determined by a temperature probe inserted into a dummy cuvette containing the standard melting buffer (TEA).

Analysis of Thermal Melting Profiles. Cary 1 report files were converted from percent transmittance to absorbance and treated as previously described (*35*). The data sets were smoothed over a 4 °C window and the melting profile presented as the derivative of absorbance with respect to temperature and plotted as a function of temperature. The data presented here are fit to a sequential folding model described in detail previously (*35*).

Analysis of Trivalent Cation Concentration Dependence of the Melting Profiles. $Co(NH_3)_6^{3+}$ titration data were fit to the equation derived by Nixon et al. (*18*). The model assumes an electrostatic interaction of one $Co(NH_3)_6^{3+}$ ion for every three phosphates. This model also assumes two-state unfolding associated with the transition being fit. For the data presented here, the number of phosphates involved in a given unfolding process was held constant at 6. The model generates RNA−metal affinities, associated with a given transition, for the folded form K_f and the unfolded form K_u (*36, 37*).

Analysis of Circular Dichroism (CD) Data. CD data were obtained using an AVIV 62DS circular dichroism spectrometer (AVIV) at a constant temperature of 25 °C. The data were taken in a 0.1 cm path length quartz cuvette at an RNA concentration of 20 μM. Data were collected from 200 to 320 nm at 1 nm intervals. The data are presented as the average of six scans for each sample, smoothed for presentation. For titration analyses, the ellipticity data were converted to molar circular dichroism (ΔE) using eq 2, where θ is the CD amplitude in millidegrees, C is the sample concentration,

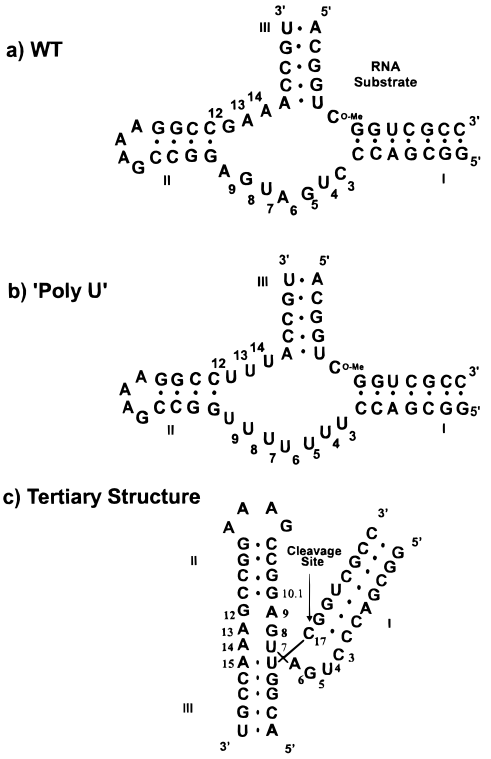

FIGURE 1: Hammerhead models used in this study. (a) WT hammerhead; (b) 'poly U' hammerhead in which the nucleotides of the conserved core are substituted with uracil. (c) Representation of the tertiary structure of the hammerhead ribozyme as predicted by X-ray crystallography (*28*).

Table 1: Relative Affinities of Mn^{2+} and $Co(NH_3)_6^{3+}$ for the Hammerhead Ribozyme

sample[a]	n_1	$K_{d(1)}$ (μM)	n_2	$K_{d(2)}$ (μM)
RNA−RNA (2′-OMe) hammerhead[b]	2.5 ± 0.9	3.3 ± 2.7	7.1 ± 0.7	122 ± 48
RNA−DNA hammerhead[c]	3.7 ± 0.4	4.0 ± 1.0	5.2 ± 0.4	461 ± 130
RNA−RNA (2′-OMe) $Co(NH_3)_6^{3+}$ competition[d]	−	22 ± 4.2	−	−

[a] Titrations performed with RNA concentrations of 1−20 μM in standard buffer conditions of 5 mM TEA, pH 7.8, 100 mM NaCl. [b] Hammerhead sequence shown in Figure 1a. [c] Reference (*24*). [d] $K_{d\ app}$ value for $Co(NH_3)_6^{3+}$ in the presence of 500 μM Mn^{2+}, as described under Materials and Methods.

L is the cell path length, and n is the number of nucleotides in the RNA.

$$\Delta E = \frac{\theta}{(32980 \times C \times L \times n)} \quad (2)$$

These data were then fit directly to eq 3 (*43*).

$$CD_{sig} = \frac{a \times [Co(NH_3)_6^{3+}]}{(K_{d\ app} + [Co(NH_3)_6^{3+}] + b)} \quad (3)$$

In eq 3, a is equal to the total change in signal amplitude and b is equal to the signal amplitude at the beginning of the titration. $K_{d\ app}$ equals the dissociation constant for $Co(NH_3)_6^{3+}$ under the conditions of the titration, and CD_{sig} is the molar absorptivity at a given $Co(NH_3)_6^{3+}$ concentration. This analysis assumes a Hill coefficient of 1 and does not assume a given number of binding events.

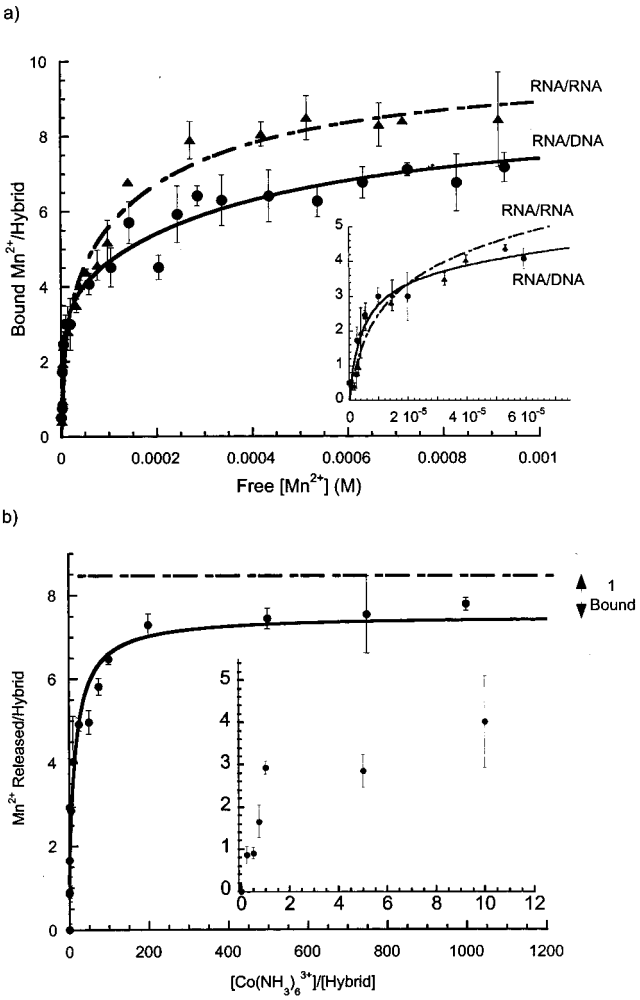

FIGURE 2: Mn^{2+} EPR binding isotherms and competition by $Co(NH_3)_6^{3+}$. (a) Room-temperature Mn^{2+} EPR binding isotherms for 1−20 μM RNA/RNA hybrid (triangles) and RNA/DNA hybrid (circles) (*24*). Data are plotted as Mn^{2+} bound/hybrid as a function of 'free' Mn^{2+}. The line through the data represents the nonlinear least-squares fit to two types of sites. The inset shows the similarity of the data for each titration at low concentrations of Mn^{2+}. (b) Plot of Mn^{2+} released/hybrid as a function of equivalents of added $Co(NH_3)_6^{3+}$. Data were taken in 500 μM Mn^{2+} and 10 μM hybrid and fit to eq 1. The inset shows release of ~3 Mn^{2+} ions with addition of 1 equiv of $Co(NH_3)_6^{3+}$.

RESULTS

Mn^{2+} Affinities for the RNA−RNA Hammerhead Ribozyme and $Co(NH_3)_6^{3+}$ Competition. Figure 2a shows the Mn^{2+} binding isotherm for the hammerhead ribozyme of Figure 1a with either an all-DNA substrate strand (RNA/DNA) or an all-RNA substrate strand (RNA/RNA) with a 2′-O-Me at the cleavage site, obtained using Mn^{2+} EPR measurements as previously described (*24*). The data for the RNA/RNA hammerhead fit well to two types of noninteracting sites with $K_{d1} = 3.3 \pm 2.7$ μM, $n = 2.5 \pm 0.9$ and $K_{d2} = 122 \pm 48$ μM, $n = 7.1 \pm 0.7$ (Table 1). These results are similar to those previously obtained for the RNA/DNA hammerhead, with the RNA/RNA hammerhead having higher average affinity for the second, weaker class of sites. To obtain an apparent affinity of $Co(NH_3)_6^{3+}$ for the hammerhead, the intensity of the Mn^{2+} EPR signal was monitored as a function of added $Co(NH_3)_6^{3+}$. As $Co(NH_3)_6^{3+}$ is added to the RNA/RNA hammerhead sample containing 500 μM Mn^{2+}, the intensity of the EPR signal due to unbound Mn^{2+} increases,

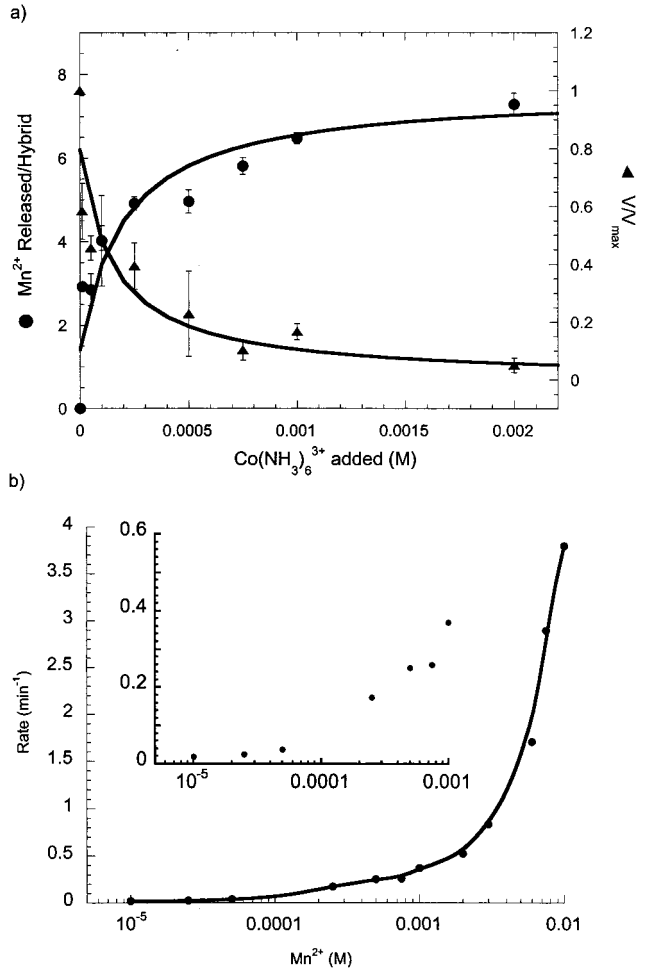

FIGURE 3: Effects of $Co(NH_3)_6^{3+}$ on WT hammerhead activity. (a) Comparison of decrease in V/V_{max} (triangles) in the presence of 500 μM Mn^{2+} and the release of bound Mn^{2+} (circles) as a function of added $Co(NH_3)_6^{3+}$. Data are fit as described under Materials and Methods to yield a $K_i[Co(NH_3)_6^{3+}]$ of $\sim 31 \pm 2$ μM and a $K_{d\ app}$ of 22 ± 4 μM, respectively. (b) Mn^{2+} rescue of hammerhead activity in 2 mM $Co(NH_3)_6^{3+}$. A smooth line is drawn through the data points for presentation.

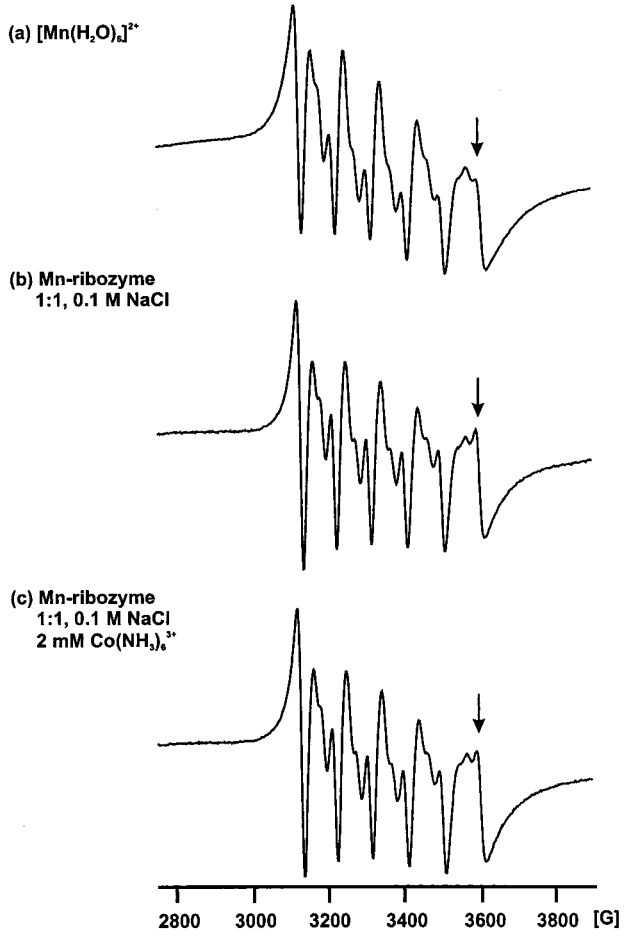

FIGURE 4: Low-temperature EPR measurements of Mn^{2+} bound to the hammerhead ribozyme. (a) 500 μM Mn^{2+}. (b) 500 μM Mn^{2+}/500 μM RNA/RNA (O-Me) hybrid. (c) 500 μM Mn^{2+}/500 μM hybrid/2 mM $Co(NH_3)_6^{3+}$. All samples are in TEA buffer, 0.1 M NaCl, and 20% ethylene glycol. EPR parameters: 10 K, 15 G ptp field modulation, 0.063 mW microwave power, 9.44 GHz, and 1 scan (*27*).

indicating release of Mn^{2+} from the hammerhead (Figure 2b). These data were fit to a simple model to obtain an apparent K_d for $Co(NH_3)_6^{3+}$ in the presence of 500 μM Mn^{2+} of $K_{d\ app} = 22 \pm 4.2$ μM.

Although the data fit well to a single $K_{d\ app}$, two aspects of the $Co(NH_3)_6^{3+}$ competition are unusual. As shown in the inset of Figure 2b, approximately 3 Mn^{2+} ions are released upon addition of the first equivalent of $Co(NH_3)_6^{3+}$. These data, obtained at 10 μM RNA concentration, indicate that there is a high-affinity $Co(NH_3)_6^{3+}$ site whose population causes release of multiple Mn^{2+} ions. The second unusual result is that one Mn^{2+} ion appears to remain bound to the hammerhead even at concentrations of up to 10 mM $Co(NH_3)_6^{3+}$. The site for this Mn^{2+} is considered in a later section.

Hammerhead Activity in the Presence of $Co(NH_3)_6^{3+}$. To directly compare the Mn^{2+} binding studies with activity measurements, identical conditions were used except that the activity measurements require a 2′-OH at the cleavage site. The observed rate of single-turnover hammerhead activity in 1 mM $Co(NH_3)_6^{3+}$ (0.1 M NaCl) in the absence of added Mn^{2+} is <0.001 min^{-1} with no cleavage observed after 24 h in these solution conditions. When the rate of hammerhead activity in 500 μM Mn^{2+} is measured as a function of added $Co(NH_3)_6^{3+}$ (Figure 3a), a 15-fold reduction in rate from 2.7 to 0.18 min^{-1} is observed with addition of up to 2 mM $Co(NH_3)_6^{3+}$. The final percent of cleaved product does not change over this range of $Co(NH_3)_6^{3+}$ concentration, indicating that the rate of 0.18 min^{-1} reflects an active, but slow hammerhead in the presence of ≥ 2 mM $Co(NH_3)_6^{3+}$ and 500 μM Mn^{2+}. At higher concentrations of up to 10 mM $Co(NH_3)_6^{3+}$ and 500 μM Mn^{2+}, no further reduction in rate is observed.

The rate data obtained as a function of added $Co(NH_3)_6^{3+}$ were fit to a simple competition model, to yield an apparent inhibition constant of $K_{i\ app} = 30.9 \pm 2.3$ μM in 500 μM Mn^{2+} (0.1 M NaCl) (Figure 3a). Comparing the Mn^{2+} competition data with the rate data shows that the loss of bound Mn^{2+} ions is closely correlated to the initial reduction in rate (Figure 3a).

To investigate the 'slow' rate supported by a mixture of Mn^{2+} and $Co(NH_3)_6^{3+}$, hammerhead activity was measured in 2 mM $Co(NH_3)_6^{3+}$ as a function of added Mn^{2+}. Figure 3b shows this titration, in which a rise in the rate from 0.002 to 0.18 min^{-1} between 10 and ~ 250 μM Mn^{2+} is observed (inset, Figure 3b). At Mn^{2+} concentrations above 5 mM, the

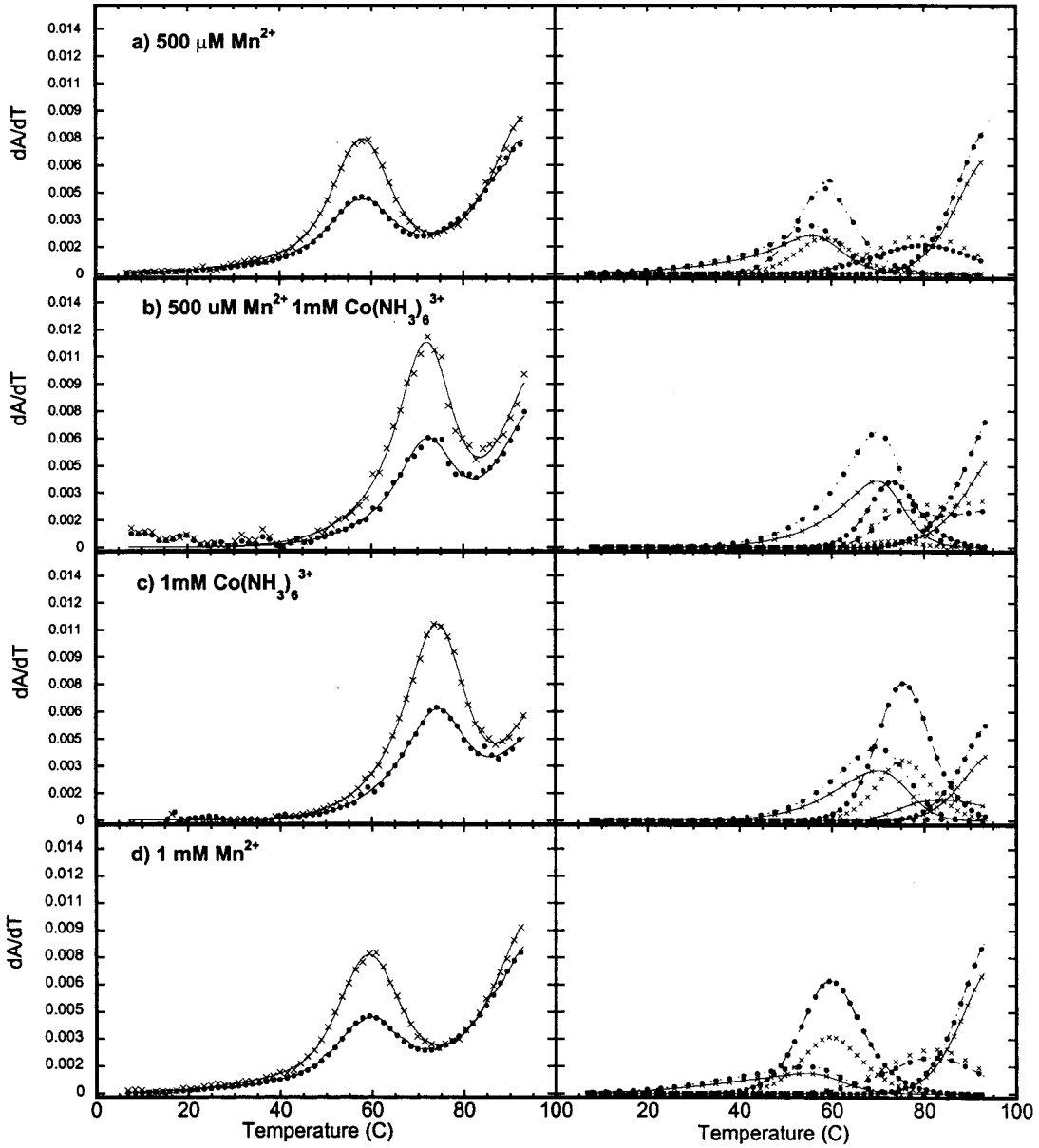

FIGURE 5: Melting profiles of WT hammerhead. Melting profiles are plotted as the derivative of absorbance with respect to temperature versus temperature. Data are taken at 260 nm (circles) and 280 nm (crosses). The line represents a nonlinear least-squares fit to the data from the addition of four sequential unfolding transitions. The panel to the right of each melting profile shows the deconvolution of the individual transitions that make up the fit. Samples are 3 μM RNA/RNA (O-Me) hammerhead in TEA buffer. (a) 500 μM Mn^{2+}, (b) 500 μM Mn^{2+} and 1 mM $Co(NH_3)_6^{3+}$, (c) 1 mM $Co(NH_3)_6^{3+}$, and (d) 1 mM Mn^{2+}.

rate increases, reaching WT levels of ~4.7 min^{-1} at 10 mM Mn^{2+} and 2 mM $Co(NH_3)_6^{3+}$. The return of activity is consistent with a reversible process in which $Co(NH_3)_6^{3+}$ may compete with Mn^{2+} for a common site in the hammerhead ribozyme.

Low-Temperature Mn^{2+} EPR Spectra in the Presence of $Co(NH_3)_6^{3+}$. The experiments described above indicate that with 500 μM Mn^{2+} and up to 10 mM $Co(NH_3)_6^{3+}$, the hammerhead ribozyme retains activity and also retains a single tightly bound Mn^{2+} ion. To investigate the nature of this bound Mn^{2+} ion, low-temperature EPR spectra were obtained of a 1:1 hammerhead/Mn^{2+} sample in the presence of $Co(NH_3)_6^{3+}$. Previously we reported a small but consistent line shape signature for Mn^{2+} bound in the highest affinity hammerhead site, which is predicted to be the A9/G10.1 site on the basis of ESEEM and ENDOR spectroscopic data (*26, 27*). This EPR line shape signature is pointed out by the arrow in Figure 4, indicating the small but reproducible difference between Mn^{2+} in buffer (Figure 4a) in comparison with a 1:1 WT hammerhead/Mn^{2+} sample (Figure 4b). This same spectral signature is observed for Mn^{2+} in the hammerhead sample containing 2 mM $Co(NH_3)_6^{3+}$ (Figure 4c). These data strongly suggest that the Mn^{2+} site that remains populated in the presence of $Co(NH_3)_6^{3+}$ is the same as that previously investigated by other spectroscopic techniques (*26, 27*), which is probably the A9/G10.1 site.

Thermal Denaturation of the Hammerhead Ribozyme as a Function of Added $Co(NH_3)_6^{3+}$. In an effort to understand the potential structural effects of $Co(NH_3)_6^{3+}$ on the hammerhead ribozyme, thermal denaturation studies were performed. Figure 5 (a−d) shows representative melting profiles for the hammerhead ribozyme at various metal concentrations. These data are shown as the derivative of absorbance with respect to temperature. The melting profile of the

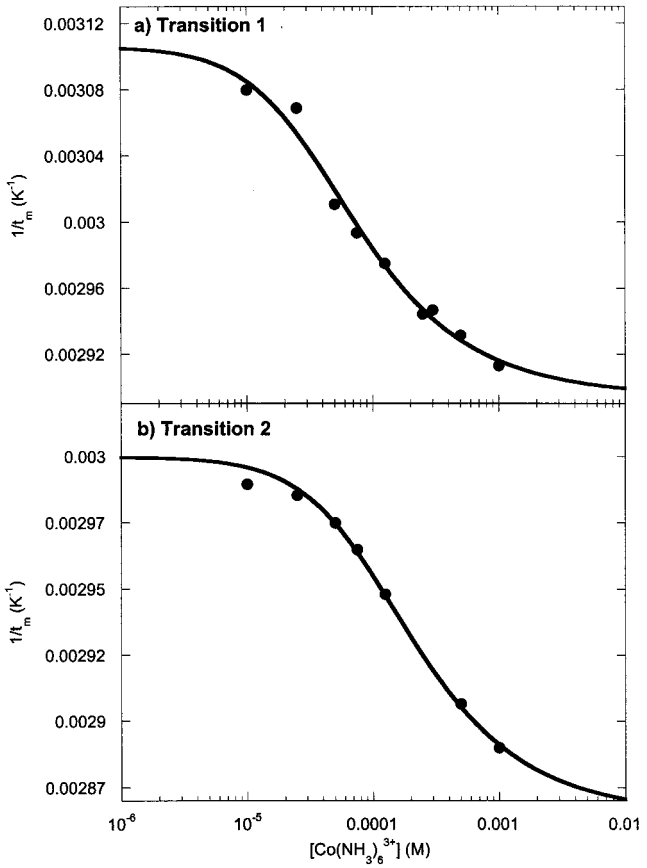

FIGURE 6: Determination of $Co(NH_3)_6^{3+}$ affinities from thermal denaturation experiments. Effect of the addition of $Co(NH_3)_6^{3+}$ in 500 μM Mn^{2+} on the melting temperature of transitions 1 and 2. (a) Plot of $1/t_m$ versus added $Co(NH_3)_6^{3+}$ for transition 1. The line through the data represents a nonlinear least-squares fit to the data as described in Nixon et al. (*18*). (b) Plot of $1/t_m$ versus added $Co(NH_3)_6^{3+}$ for transition 2.

hammerhead in 500 μM Mn^{2+} is characterized by two large derivative features, one centered at about 60 °C and the other at ~90 °C. The transition at 90 °C can be unambiguously assigned to the unfolding of the GAAA tetraloop in combination with stem II (*38*−*40*). The smooth curve through the data represents a best-fit line that is the sum of four sequential two-state unfolding curves. The panel to the right of the data is the deconvolution of the individual transitions that make up the fit to the data. The large feature at 60 °C can be deconvoluted into three sequential unfolding events, for which the first two are tentatively assigned (*40*) to include unfolding of stems I and III and associated tertiary structure. Addition of 1 mM $Co(NH_3)_6^{3+}$ in 500 μM Mn^{2+} leads to an increase in the t_m of this main transition to a t_m ~ 70 °C (Figure 5b), consistent with stabilization of the stem I and III duplexes and associated tertiary structure with added trivalent ions.

A measure of the relative affinities for $Co(NH_3)_6^{3+}$ to the hammerhead ribozyme in the presence of 500 μM Mn^{2+} can be calculated by applying an electrostatic model for the association of trivalent cations with RNA to the increase in t_m obtained as a function of added $Co(NH_3)_6^{3+}$ (*18*). $Co(NH_3)_6^{3+}$ affinities for both the folded (K_f) and unfolded (K_u) forms of the RNA associated with the first two transitions were determined in this manner (Figure 6 a,b). For transitions 1 and 2, affinities of $K_{f1} = 12\,190 \pm 1206$ (M^{-1}) ($K_{d1} = 82$ μM) and $K_{u1} = 3703 \pm 478$ (M^{-1}) and $K_{f2} = 4404 \pm 326$ (M^{-1}) ($K_{d2} = 227$ μM) and $K_{u2} = 1367 \pm 145$ (M^{-1}) were found, respectively. The K_{d1} of 82 μM, based on this electrostatic model for transition 1, is similar to the $K_{i\ app}$ of 31 μM observed in the activity studies. This suggests a correlation between the observed thermal stabilization, the loss of activity, and the displacement of bound Mn^{2+} with the addition of $Co(NH_3)_6^{3+}$. The apparent $Co(NH_3)_6^{3+}$ affinities derived from these transitions can be compared directly to the affinities calculated in the same manner for Mn^{2+} alone (data not shown). The Mn^{2+} affinities reflect the slightly weaker binding of divalent ions compared to that of the trivalent $Co(NH_3)_6^{3+}$ with $K_f = 9874$ (M^{-1}) ($K_{d1} = 101$ μM) and $K_f = 1169$ (M^{-1}) ($K_{d2} = 890$ μM) for transitions 1 and 2, respectively (*40*).

Of interest is the melting profile of the hammerhead in 1 mM $Co(NH_3)_6^{3+}$ in the absence of Mn^{2+}. In this sample the t_m of the main feature is increased further to ~75 °C (Figure 5c). The lower t_m in 500 μM Mn^{2+} and 1 mM $Co(NH_3)_6^{3+}$ in comparison with $Co(NH_3)_6^{3+}$ alone is reflected by a free energy difference for transition 2 of $\Delta(\Delta G_{37°C}) = +0.5$ kcal mol^{-1}, and indicates that addition of Mn^{2+} slightly destabilizes the $Co(NH_3)_6^{3+}$-bound form of the hammerhead ribozyme. Under these conditions, the activity has reached a slow value and a single Mn^{2+} ion remains tightly bound. In 1 mM Mn^{2+} alone, the main transition occurs at a lower t_m than in 1 mM $Co(NH_3)_6^{3+}$ (Figure 5d), consistent with the increased stabilization of RNA duplexes by trivalent cations compared with that of divalent cations (*18*).

Circular Dichroism Spectroscopy of the Hammerhead Ribozyme. Circular dichroism (CD) spectroscopy has been shown to be an effective method to investigate RNA conformation (*41*, *42*). In recent studies, CD spectroscopy has been used to determine the presence of folding intermediates in the RNase P RNA upon addition of Mg^{2+} (*43*, *44*). Here, circular dichroism spectra were measured for the hammerhead ribozyme in an attempt to correlate possible structural changes with the addition of $Co(NH_3)_6^{3+}$ or Mn^{2+}. CD spectra of the hammerhead enzyme/substrate complex are characterized by a large positive ellipticity with a maximum at 266 nm and a small negative band at 230 nm (Figure 7). The spectrum of the 34 nt 'enzyme' strand (Figure 7a, dotted line) is also shown which clearly shows that a distinctive CD spectrum is obtained upon hybrid formation.

Figure 7a shows the change in the CD spectra of the hammerhead ribozyme observed with the addition of $Co(NH_3)_6^{3+}$. Upon addition of $Co(NH_3)_6^{3+}$, an increase in ellipticity at 266 nm is observed accompanied by a concurrent decrease in ellipticity at 230 nm. Fitting the change in the molar ellipticity as a function of added $Co(NH_3)_6^{3+}$ at these two wavelengths yields different K_d values for each wavelength (Figure 8a, Table 2). For the transition at 230 nm, a value of $K_d = 266 \pm 55$ μM can be calculated for association of $Co(NH_3)_6^{3+}$, and for the transition at 266 nm, a value of $K_d = 43 \pm 16$ μM is found. These two wavelengths appear to be reporting on two separate events that are occurring upon $Co(NH_3)_6^{3+}$ binding, which result in the observed CD spectra. Mn^{2+} addition to the hammerhead ribozyme also results in an increase in ellipticity at 266 nm, but unlike for the $Co(NH_3)_6^{3+}$ titration, no large change is observed at 230 nm (Figure 7b). The Mn^{2+}-induced increase in molar ellipticity at 266 nm can be fit to find a K_d of ~476 ± 126 μM (Table 2). A similar titration with Mg^{2+} did not show

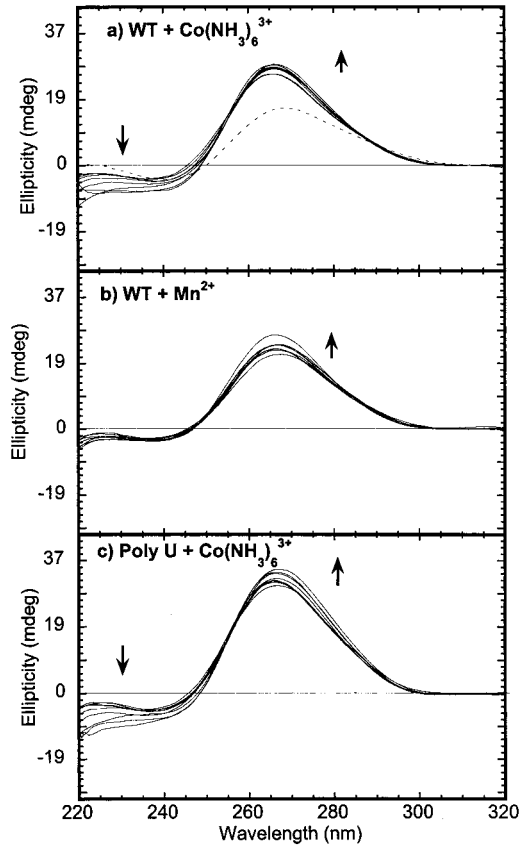

FIGURE 7: Circular dichroism (CD) spectroscopy of the WT and 'poly U' hammerheads as a function of added Mn^{2+} or $Co(NH_3)_6^{3+}$. CD spectra are plotted as ellipticity (millidegrees) versus wavelength (nanometers). Lines represent smooth curves through the average of six separate scans taken at 1 nm intervals from 220 to 320 nm. (a) WT hammerhead (20 μM) with addition of 0−3 mM $Co(NH_3)_6^{3+}$. Also shown is the CD spectrum of the 34 nt 'enzyme' strand alone (dashed line). (b) WT hammerhead with addition of 0−10 mM Mn^{2+}. (c) 'poly U' hammerhead with addition of 0−3 mM $Co(NH_3)_6^{3+}$.

the change in ellipticity at 230 nm, but it did show similar changes at 266 nm (data not shown).

In an attempt to define the specific interactions associated with $Co(NH_3)_6^{3+}$ binding to the hammerhead ribozyme, a mutant hammerhead was studied. The 'poly U' hammerhead contains uracil residues at each of the conserved sites in the hammerhead core (Figure 1b). The 'poly U' hammerhead lacks the required residues to form the core domains associated with proper folding, but retains the ability to form the three stems. Titrating this hammerhead with $Co(NH_3)_6^{3+}$ induces a change in CD features at 230 and 266 nm (Figure 7c), as observed for the WT hammerhead. However, for the 'poly U' hammerhead, the dissociation constant derived for the CD change at 266 nm is $K_d = 140 \pm 59$ μM, which is a 4-fold decrease from the affinity obtained for the WT hammerhead (Figure 8b). This suggests that in the WT hammerhead the transition at 266 nm may be reporting on metal binding to nucleotides in the hammerhead core as well as helices in the stems. The derived dissociation constant for the $Co(NH_3)_6^{3+}$-induced CD signal at 230 nm is 265 ± 52 μM. The similar $Co(NH_3)_6^{3+}$ affinities derived from this transition in the WT and 'poly U' hammerheads (Figure 8b) suggest that the induced CD feature at 230 nm is reporting on nonspecific interactions of $Co(NH_3)_6^{3+}$ with the A-form helices in the RNA. Consistent with this, $Co(NH_3)_6^{3+}$ titration

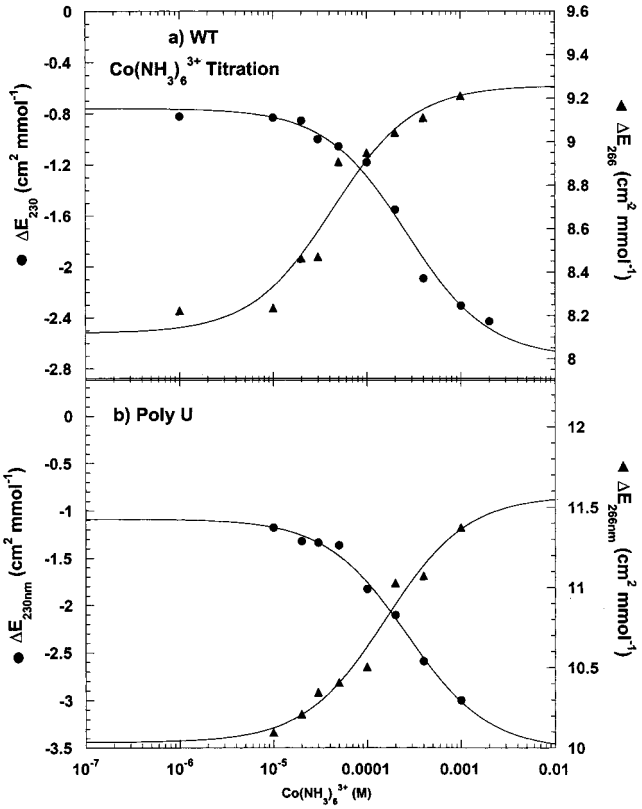

FIGURE 8: $Co(NH_3)_6^{3+}$ binding curves obtained from CD data. (a) Titration curves for the WT hammerhead as a function of added $Co(NH_3)_6^{3+}$. Molar ellipticity is plotted versus added $Co(NH_3)_6^{3+}$ at two wavelengths, 230 nm (circles) and 266 nm (triangles). The line through the data represents a fit to eq 3 as described in (*43*), yielding K_d values for $Co(NH_3)_6^{3+}$. (b) Titration curves for 'poly U' hammerhead as a function of added $Co(NH_3)_6^{3+}$.

Table 2: Metal Affinities for Hammerhead Ribozyme Derived from CD Spectroscopy

sample[a]	K_d(266 nm)	K_d(230 nm)
WT hammerhead		
$Co(NH_3)_6^{3+}$	43 ± 16 μM	266 ± 55 μM
Mn^{2+}	476 ± 126 μM	N/A
'poly U' hammerhead		
$Co(NH_3)_6^{3+}$	140 ± 59 μM	265 ± 52 μM

[a] Titrations performed with a sample concentration of 20 μM in standard buffer conditions of 5 mM TEA, pH 7.8, 100 mM NaCl.

of a 13 nucleotide RNA duplex shows similar induced CD spectra as a function of added $Co(NH_3)_6^{3+}$ (data not shown).

DISCUSSION

The consequences of addition of $Co(NH_3)_6^{3+}$ to the hammerhead ribozyme have been followed by activity measurements, Mn^{2+} binding profiles, thermal denaturation studies, and CD spectroscopy. The results of these studies are summarized in Table 3. In general, each of these experiments reports on at least two types of ion-binding sites in the hammerhead which have distinguishable apparent dissociation constants. The apparent K_i of 31 μM that describes $Co(NH_3)_6^{3+}$ inhibition of hammerhead activity is generally matched by the higher affinity $Co(NH_3)_6^{3+}$ interactions reported on by each of these experiments. A weaker affinity for $Co(NH_3)_6^{3+}$ also is observed which may be due to nonspecific binding of this ion to RNA duplexes.

Table 3: Summary of Apparent $Co(NH_3)_6^{3+}$ Affinities for the Hammerhead Ribozyme

K_i[a]	30.9 ± 2.3 μM	
$K_{d\ app}$[b]	22.1 ± 4.2 μM	
$K_{d\ f1,2}$[c]	82.0 ± 8.1 μM	227 ± 16.8 μM
$K_{d\ (266,230)}$[d]	43.0 ± 16.0 μM	266 ± 55 μM

[a] Inhibition constant in the presence of 500 μM Mn^{2+}. [b] Apparent K_d in the presence of 500 μM Mn^{2+}. [c] Derived from thermal denaturation experiments. [d] Derived from CD measurements.

These results, taken together, suggest that population of a specific high-affinity site(s) for $Co(NH_3)_6^{3+}$ in the hammerhead ribozyme causes inhibition of activity. Population of this (these) site(s) by $Co(NH_3)_6^{3+}$ is associated with structural changes that are characterized by release of more than one bound Mn^{2+} ion and an increase in the CD signature at 266 nm. One candidate for this inhibitory site is the G5 site that has previously been found to bind Tb^{3+} and Eu^{3+} with apparent high affinity (*21*). Hammerhead inhibition by Tb^{3+} and Eu^{3+} is believed to be due to inner-sphere contacts between these ions and the binding face of the G5 residue. It has been suggested that in Mg^{2+}-supported activity, the divalent ion bound at this G5 site may be released upon formation of the transition state. This inhibition by trivalent ions is suggested to be due to their higher affinity and thus more sluggish release from this site. $Co(NH_3)_6^{3+}$ has been reported to 'efficiently' compete with both Tb^{3+} and Eu^{3+} for binding at the G5 site (*21*). Because $Co(NH_3)_6^{3+}$ is ligand-exchange-inert, it may be expected to have a weaker affinity for this site. Consistent with this, the observed K_i for $Co(NH_3)_6^{3+}$ is ~10-fold weaker ($K_i \sim 31$ μM, 500 μM Mn^{2+}, 0.1 M NaCl), than those reported for Tb^{3+} ($K_i \sim 1$ μM, 10 mM $MgCl_2$) (*21*).

It is intriguing that a residual, but slow, activity of the hammerhead is maintained in mixtures of $Co(NH_3)_6^{3+}$ and Mn^{2+}. Even with high levels of added $Co(NH_3)_6^{3+}$, a single Mn^{2+} site is populated which may be responsible for the residual hammerhead activity. This site is likely the A9/G10.1 site based on its low-temperature Mn^{2+} EPR signature (Figure 4) (*27*), and the known inner-sphere phosphate and nitrogen ligands predicted for this site by X-ray crystallography and spectroscopic measurements (*26*−*28*). Inner-sphere coordination of Mn^{2+} at the A9/G10.1 site would explain why the exchange-inert $Co(NH_3)_6^{3+}$ is unable to efficiently compete for the site. The observed residual activity in the presence of a single bound Mn^{2+} is consistent with the known requirement of metal ion population at the A9/G10.1 site, and supports recent proposals that the A9/G10.1 site may indeed play a major role in the catalytic activity of the hammerhead ribozyme (*4, 31, 32*).

If it is assumed that the same cleavage mechanism operates in the presence and absence of $Co(NH_3)_6^{3+}$, the effects of $Co(NH_3)_6^{3+}$ suggest that at least two types of divalent metal ion sites govern hammerhead activity. The slowed rate of the reaction in the combination of $Co(NH_3)_6^{3+}$ and low concentrations of Mn^{2+} must be due to $Co(NH_3)_6^{3+}$ population of another site in addition to Mn^{2+} population of the A9/G10.1 site. This inhibition by $Co(NH_3)_6^{3+}$ can in turn be relieved by increasing concentrations of Mn^{2+}, which suggests that Mn^{2+} populates the site at which $Co(NH_3)_6^{3+}$ binds. Alternatively, Mn^{2+} may relieve $Co(NH_3)_6^{3+}$ inhibition by populating an additional site which either has a reduced Mn^{2+} affinity in the presence of $Co(NH_3)_6^{3+}$, or whose population releases the bound and inhibitory $Co(NH_3)_6^{3+}$. Either way, these results suggest the presence of at least two metal ion sites whose population by Mn^{2+} or other divalent cations is critical in the hammerhead reaction: the A9/G10.1 site and also at least one additional site. A likely candidate for the additional site is the G5 site, but other possibilities cannot be ruled out by these analyses.

Also of interest is the release of 2−3 Mn^{2+} ions from the hammerhead upon addition of a single equivalent of $Co(NH_3)_6^{3+}$. Lilley and co-workers have suggested that $Co(NH_3)_6^{3+}$ inhibits a folding event (*20*) later associated with the formation of the CUGA turn in their predicted hammerhead folding pathway (*5*). Given this, the release of 2−3 Mn^{2+} ions may be due to disruption by $Co(NH_3)_6^{3+}$ of this CUGA turn and thus the folding of Domain I in the hammerhead core. These results are consistent with observations that the 'poly-U' hammerhead and also an A14-G mutant hammerhead, both of which should be defective in core folding, also lack the majority of high-affinity Mn^{2+} sites (*45*).

Relevant to the proposal here that $Co(NH_3)_6^{3+}$ binding induces a local structural change and release of multiple Mn^{2+} ions, Yoshinari and Taira (*31*) recently have concluded that binding of Cd^{2+} to the A9/G10.1 site causes release of two Mg^{2+} or Ca^{2+} ions. Their proposal also requires that local structural rearrangements are induced upon filling a specific metal site in the hammerhead.

In addition to the inhibitory and structural effects on the hammerhead caused by low concentrations of $Co(NH_3)_6^{3+}$, both thermal denaturation and CD measurements suggest a lower affinity binding of $Co(NH_3)_6^{3+}$ to the RNA duplex regions of the hammerhead. The CD signature at 230 nm, observed upon addition of $Co(NH_3)_6^{3+}$ to the WT hammerhead, the poly-U hammerhead, and an RNA/RNA duplex, appears to be reporting on $Co(NH_3)_6^{3+}$ binding to duplex RNA regions with a K_d of ~265 μM. This affinity correlates well with the stabilization by $Co(NH_3)_6^{3+}$ of transition 2 in the hammerhead melt profiles (Table 3). A CD signal at 230 nm has previously been reported with addition of $Co(NH_3)_6^{3+}$ to duplex DNA (*46*), and attributed to formation of a more highly stacked conformation. The same explanation may hold for duplex RNA.

In summary, the results obtained by following the $Co(NH_3)_6^{3+}$-induced inhibition of hammerhead activity emphasize the sensitivity of hammerhead ribozyme activity to metal ion interactions. The mechanism of $Co(NH_3)_6^{3+}$ inhibition appears to be due to a specific high-affinity binding event which subtly alters the structure of the hammerhead. Residual slow activity in the presence of low concentrations of Mn^{2+} ions suggests that at least one site with inner-sphere metal ion interactions is required for activity, and that binding of the trivalent $Co(NH_3)_6^{3+}$ to an additional site is the cause of the slowed rate. Because higher concentrations of Mn^{2+} can reverse the effects of $Co(NH_3)_6^{3+}$, it is suggested that population of at least two specific metal ion sites by divalent cations is required for efficient hammerhead cleavage activity in 0.1 M NaCl.

ACKNOWLEDGMENT

We thank Professor David P. Giedroc for the use of his optical melt instrumentation. Dr. Jon Christopher developed

the fitting program (T-Melt) for the optical data. We also thank Dr. Iddys Figueroa for assistance in the use of the CD spectrometer and for helpful discussion.

REFERENCES

1. Uhlenbeck, O. C. (1987) *Nature 328*, 596−600.
2. Dahm, S. C., Derrick, W. B., and Uhlenbeck, O. C. (1993) *Biochemistry 32*, 13040−13045.
3. Misra, V. K., and Draper, D. E. (1999) *Biopolymers 48*, 113−135.
4. Wang, S., Karbstein, K., Peracchi, A., Beigelman, L., and Herschlag, D. (1999) *Biochemistry 38*, 14363−14378.
5. Bassi, G. S., Mollegaard, N. E., Murchie, A. I. H., and Lilley, D. M. J. (1999) *Biochemistry 38*, 3345−3354.
6. Scott, E. C., and Uhlenbeck, O. C. (1999) *Nucleic Acids Res. 27*, 479−484.
7. Cowan, J. A. (1993) *J. Inorg. Biochem. 49*, 171−175.
8. Young, K. J., Gill, F., and Grasby, J. A. (1997) *Nucleic Acids Res. 25*, 3760−3766.
9. Hampel, A., and Cowan J. A. (1997) *Chem. Biol. 4*, 513−517.
10. Murray, J. B., Seyhan, A. A., Walter, N. G., Burke, J. M., and Scott, W. G. (1998a) *Chem. Biol. 5*, 587−595.
11. Cate, J. H., Gooding, A. R., Podell, E., Zhou, K. H., Golden, B. L., Kundrot, C. E., Cech, T. R., and Doudna, J. A. (1996) *Science 273*, 1678−1685.
12. Kieft, J. S., and Tinoco, I. (1997) *Structure 5*, 713−721.
13. Rudisser, S., and Tinoco I. (2000) *J. Mol. Biol. 295*, 1211−1223.
14. Gonzales, R. L., and Tinoco, I. (1999) *J. Mol. Biol. 289*, 1267−1282.
15. Butcher, S. E., Allain, F. H. T., and Feigon J. (2000) *Biochemistry 39*, 2174−2182.
16. Maderia, M., Horton, T. E., and DeRose, V. J. (2000) *Biochemistry 39*, 8193−8200.
17. Gdaniec, Z., Sierzputowska-Gracz, H., and Theil, E. C. (1998) *Biochemistry 37*, 1505−1512.
18. Nixon, P. L., Theimer, C. A., and Giedroc, D. P. (1999) *Biopolymers 50*, 443−458.
19. Gessner, R. V., Quigley, G. J., Wang, A. H. J., van der Marel, G. A., van Boom, J. H., and Rich, A. (1985) *Biochemistry 24*, 237−240.
20. Bassi, G. S., Mollegaard, N. E., Murchie, A. I. H., von Kitzing, E., and Lilley, D. M. J. (1995) *Struct. Biol. 2*, 45−55.
21. Feig, A. L., Panek, M., Horrocks, W. D., and Uhlenbeck O. C. (1999) *Chem. Biol. 6*, 801−810.
22. Feig, A. L., Scott, W. G., and Uhlenbeck O. C. (1998) *Science 279*, 81−84.
23. Lott, W. B., Pontius, P. W., and Von Hippel P. H. (1998) *Proc. Natl. Acad. Sci. U.S.A. 95*, 542−547.
24. Horton, T. E., Clardy, D. R., and DeRose, V. J. (1998) *Biochemistry 37*, 18094−18101.
25. Hunsicker, L. M., and DeRose, V. J. (2000) *J. Inorg. Chem. 80*, 271−281.
26. Morrissey, S. R., Horton, T. E., Grant, C. V., Hoogstraten, C. G., Britt, R. D., and DeRose, V. J. (1999) *J. Am. Chem. Soc. 121*, 9215−9218.
27. Morrissey, S. R., Horton, T. E., and DeRose, V. J. (2000) *J. Am. Chem. Soc. 122*, 3473−3481.
28. Pley, H. W., Flaherty, K. M., and Mckay, D. B. (1994) *Nature 372*, 68−74.
29. Scott, W. G., Finch, J. T., and Klug, A. (1995) *Cell 81*, 991−1002.
30. McKay, D. B. (1997) *RNA 2*, 395−403.
31. Yoshinari, K., and Taira, K. (2000) *Nucleic Acids Res. 28*, 1730−1742.
32. Peracchi, A., Beigelman, L., Scott, E. C., Uhlenbeck, O. C., and Herschlag, D. (1997) *J. Biol. Chem. 272*, 26822−26826.
33. Murray, J. B., and Scott, W. G. (2000) *J. Mol. Biol. 296*, 33−41.
34. Milligan, J. F., and Uhlenbeck, O. C. (1989) *Methods Enzymol. 180*, 51−62.
35. Theimer, C. A., and Giedroc, D. P. (1999) *J. Mol. Biol. 289*, 1283−1299.
36. Laing, L. G., and Draper, D. E. (1994) *J. Mol. Biol. 237*, 560−576.
37. Nixon, P. L., and Giedroc, D. P. (1998) *Biochemistry 37*, 16116−16129.
38. Heus, H. A., and Pardi, A. (1990) *Nucleic Acids Res. 18*, 1103−1108.
39. Horton, T. E., Maderia, M., and DeRose, V. J. (2000) *Biochemistry 39*, 8201−8207.
40. Horton, T. E., and DeRose, V. J. (in preparation).
41. Gray, D. M., Hung S. H., and Johnson, K. H. (1995) *Methods Enzymol. 246*, 19−34.
42. Gray, D. M., and Johnson, K. H. (1992) *J. Biomol. Struct. Dyn. 9*, 733−745.
43. Pan, T., and Sosnick, T. R. (1997) *Nat. Struct. Biol. 4*, 931−938.
44. Fang, X., Pan, T., and Sosnick, T. R. (1999) *Biochemistry 38*, 16840−16846.
45. Hunsicker, L. M., Morrissey, S. R., and DeRose, V. J. (in preparation).
46. Rodger, A., Latham, H. C., Wormell, P., Parkinson, M. I., and Sanders, K. J. (1998) *Enantiomer 3*, 395−408.

BI001141G